J Infrared Milli Terahz Waves (2011) 32:1178–1191
DOI 10.1007/s10762-011-9813-6

Plasmon Excitation and Plasmonic Detection of Terahertz Radiation in the Grating-Gate Field-Effect-Transistor Structures

Viacheslav V. Popov

Received: 31 October 2010 / Accepted: 18 July 2011 /
Published online: 30 July 2011
© Springer Science+Business Media, LLC 2011

Abstract Physics of plasma oscillations and basic principles of plasmonic detection of terahertz radiation in the grating-gate transistor structures with two-dimensional electron channels are considered. It is shown that the grating-gate-transistor plasmonic detectors can be efficiently coupled to terahertz radiation. Plasmonic detection response considerably increases if the electron density in the grating-gate transistor structure is spatially modulated.

Keywords Two-dimensional electron gas · Plasmons · Terahertz radiation · Detection · Field-effect transistor · Gratings

1 Introduction

Terahertz (THz) Plasmonics is a newly emerging field of THz physics and technology studying the processes of detection and generation of THz radiation by using plasma oscillations (plasmons) in semiconductor microdevices. Terahertz response of semiconductor microdevices with two-dimensional (2D) electron channels such as the field-effect transistors (FETs) and akin devices is strongly affected by plasma oscillations exited in the device channel. This phenomenon can be used for the detection, frequency multiplication and generation of THz radiation [1–12] as well as for THz imaging [13–16]. Plasmonic devices exhibit fast response that can be broadband or electrically tunable through the entire THz frequency band with a deep sub-THz-wavelength spatial resolution (which is important for THz near-field microscopy). The latest experimental studies have demonstrated that plasmonic THz detectors exhibit a responsivity of about 100 V/W (up to 70 kV/W with an integrated video amplifier) and the noise equivalent power of 300 pW/Hz$^{1/2}$ [15] along with a great signal transmission speed up to 10^9 cm/s [17].

V. V. Popov (✉)
Kotelnikov Institute of Radio Engineering and Electronics (Saratov Branch) RAS, 410019 Saratov, Russia
e-mail: popov@soire.renet.ru

V. V. Popov
Saratov State University, 410012 Saratov, Russia

One of the main problems to be solved with THz plasmonic devices is how to couple short-wavelength plasmon oscillations to relatively long-wavelength THz radiation (THz radiation wavelength typically exceeds the plasmon wavelength by two, or even three, orders of magnitude). Therefore, special antenna elements are needed for coupling the plasmons in a 2D electron channel to THz radiation. A metal grating gate of a relatively large area (comparable with a typical cross-section area of a focused THz beam) placed in close proximity to the 2D electron channel is an efficient coupler between plasmons and THz radiation [18–22]. Collective plasmon modes distributed over the entire area of the grating-gate structure are excited due to the constructive interference of the plasma oscillations in different unit cells of the structure. The equilibrium electron density in the 2D electron channel can be modulated along the channel by applying DC voltage to the grating-gate fingers. In this way, the frequency of a collective plasmon mode in the grating-gate structure is electrically tunable.

In this paper, the physics of plasma oscillations and basic principles of plasmonic detection of THz radiation in the grating-gate FET structures with 2D electron channels are considered. The dispersion properties of different types of plasmon modes in FET structures are described in Section 2. In Section 3, the plasmon spectra in the grating-gate FET structures are considered. Principles of plasmonic detection in the grating-gate FET structures are discussed in Section 4. The main conclusions are summarized in Section 5.

2 Plasmon dispersion

The plasmon dispersion in a 2D electron system is [23]

$$\omega = \sqrt{\frac{2\pi e^2 N q}{m^* \overline{\varepsilon}}}, \tag{1}$$

where ω and q are the plasmon frequency and wavevector, respectively, N is the sheet electron density in 2D electron system, e and m^* are the electron charge and effective mass, respectively, $\overline{\varepsilon}$ is an effective dielectric function. A particular form of the effective dielectric function depends on the geometry of the structure:

(i) If the 2D electron system is located on the surface of a substrate having the dielectric constant ε_s, then $\overline{\varepsilon} = (1 + \varepsilon_s)/2$.

(ii) If the 2D electron system is located on the surface of a substrate having the dielectric constant ε_s and covered by a barrier layer having the dielectric constant ε_b and thickness d, then

$$\overline{\varepsilon} = \frac{1}{2}\left[\varepsilon_s + \varepsilon_b \frac{1 + \varepsilon_b \tanh(qd)}{\varepsilon_b + \tanh(qd)}\right]. \tag{2}$$

[For sufficiently thick barrier layer so that $qd \gg 1$, Eq. (2) yields $\overline{\varepsilon} = (\varepsilon_s + \varepsilon_b)/2$.]

(iii) If the barrier layer is covered by a perfectly conductive plane (the gate contact), then

$$\overline{\varepsilon} = \frac{1}{2}[\varepsilon_s + \varepsilon_b \coth(qd)]. \tag{3}$$

The comparison of Eqs. (2) and (3) shows that the screening effect by the gate decreases the plasmon frequency by a factor of

$$\left(\frac{\varepsilon_b(1+\varepsilon_s)+\varepsilon_s\tanh(qd)+\varepsilon_b^2\tanh(qd)}{\varepsilon_b(1+\varepsilon_s)+\varepsilon_s\tanh(qd)+\varepsilon_b^2\coth(qd)}\right)^{1/2}<1. \tag{4}$$

For a thin barrier layer so that $qd \ll 1$, the approximation $\coth(qd) \approx 1/qd$ is valid and, hence, the plasmon spectrum given by Eq. (1) with the effective dielectric function described by Eq. (3) has a linear dispersion

$$\omega = q\sqrt{\frac{4\pi e^2 Nd}{m^*\varepsilon_b}}. \tag{5}$$

In this case, the screening factor given by Eq. (4) approximates as $[qd(1+\varepsilon_s)/\varepsilon_b]^{1/2} \ll 1$.

If a FET has the gated as well as the ungated regions of 2D electron channel (see Fig. 1), both screened and unscreened plasmons having different dispersion can exist in such FET. The wavevectors of the screened and unscreened plasmons are determined by the lengths of the gated or ungated parts of 2D electron channel, w and W, respectively. For symmetric boundary conditions at the ends of the gated or ungated sections of the channel, these wavevectors are [24] $q_n = (2n-1)\pi/w$ and $q_n = (2n-1)\pi/W$ $(n = 1, 2, 3, \ldots)$ for gated and ungated plasmons, respectively.

In actual FETs the gate-to-channel separation is typically much smaller than the gate length. In this case the electron density in the gated region of the channel (at zero drain-to-source bias) can be related to the gate voltage in a simple parallel-plate capacitor model as

$$N = \frac{\varepsilon_b}{4\pi e}\frac{U_g - U_{th}}{d},$$

where U_g is the gate voltage value and U_{th} is the channel depletion threshold voltage. Then the gated-plasmon dispersion Eq. (5) becomes [1, 2]

$$\omega = q_n\sqrt{\frac{e(U_g - U_{th})}{m^*}}. \tag{6}$$

For the gate length of 100 nm and $U_g - U_{th} = 1$V, Eq. (6) yields the fundamental (n=1) gated-plasmon mode frequency, f=$\omega/2\pi$, about 4.8 THz, 8.1 THz, and 4.2 THz for Si, GaAs, and GaN transistors, respectively.

The gated and ungated plasmons can exist independently only in idealized structures. In actual transistor structures the gated and ungated plasmons become coupled and can interact with each other. In particular, the ungated plasmons can be excited in the ungated (access)

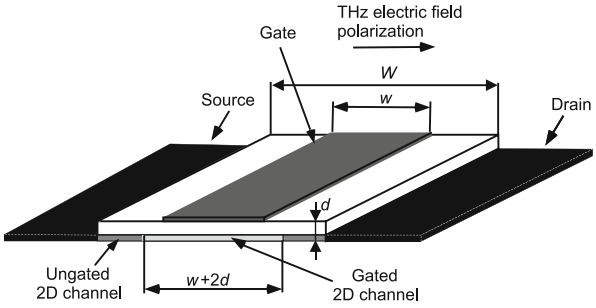

Fig. 1 Schematic of the field-effect transistor structure with 2D electron channel.

regions of the 2D electron channel as a result of the gated-plasmon scattering at the ends of the gated region of the channel [25]. This effect can cause a large broadening of the gated-plasmon resonance linewidth [26].

The gated plasmons are more attractive for practical applications because the gated-plasmon frequency can be effectively tuned by varying the gate voltage. Unfortunately, however, the gated plasmons are strongly screened by the gate contact and, hence, couple only weakly to THz radiation [25]. Due to a quadrupole-like distribution of the oscillating electric charges in the gated-plasmon mode, this plasmon mode has a very small net dipole moment, which considerably weakens the coupling between the gated plasmons and THz radiation. [The quadrupole symmetry of the gated-plasmon mode also leads to its acoustic-like spectrum described by Eqs. (5) and (6).]

3 Plasmon resonances in the grating-gate FET

The spectra and spatial waveforms of different plasmon modes in the grating-gate transistor structure (shown schematically in Fig. 2) with a homogeneous (unmodulated) 2D electron channel were considered in [27–29]. Plasmon mode excitation in the 2D electron system with a spatially modulated electron density was studied in [30–34], where the plasmon modes localized in the regions of the channel with a small electron density under the grating-gate fingers were considered. The localization of plasmon modes in depleted regions of the 2D electron channel under the grating-gate fingers leads to faster decrease of the plasmon mode frequency as compared with decreasing the average electron concentration in the structure period.

It was shown in [35] that the ungated plasmon modes in the FET sections under the grating-gate openings can also be excited in the grating-gate transistor structures. Due to coupling between the gated and ungated plasmons, complex hybrid plasmon modes are formed over the structure period.

Spatial modulation of electromagnetic properties of the grating-gate structure can be caused by (i) spatial modulation of the electron density in the 2D electron channel by applying the gate voltage and/or (ii) spatially modulated screening of the 2D electron channel by the grating-gate fingers. For a weak spatial modulation of the structure (for large gate-to-channel separation d and a homogeneous 2D electron channel), the basic parameter controlling the coupling between plasmons in the FET channel and THz radiation is the structure periodicity. In this case, the physical mechanism of plasmon excitation by incident THz wave can be explained

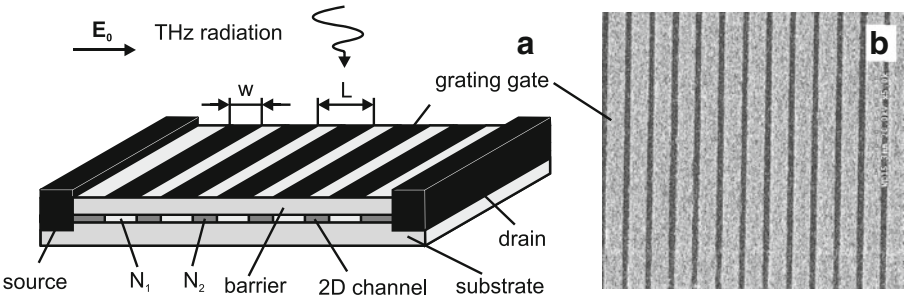

Fig. 2 Schematic of the grating-gate FET structure (left). THz radiation with polarization of the electric field across the gate fingers is incident from the top. Scanning electron microscopy image of the grating-gate fragment with period 1.5 μm and slit width 0.35 μm (right) (after Ref. [22]).

as the following. Electromagnetic wave incident upon the grating gate excites diffracted electromagnetic waves with the in-plane wavevectors $q = 2\pi p/L$ $(p = 0, \pm 1, \pm 2, ...)$, where L is the structure period. Diffracted waves with wavevectors q=0 (p=0) are virtually the reflected and transmitted electromagnetic waves traveling away from the structure. For short-period structures (with periods much shorter than the THz wavelength) which is typically the case in the grating-gate FET structures, all diffracted waves with $p \neq 0$ are the evanescent waves decaying away from the grating gate. Evanescent wave with the in-plane wavevector $q = 2\pi p/L$ excites the plasmon mode with the same wavevector in the 2D electron channel if the frequency of an incident THz wave coincides with the plasmon mode frequency. The electromagnetic coupling between the plasmons and THz radiation considerably increases for narrow openings of the grating gate because stronger spatial Fourier harmonics of the THz electric field are excited in narrower grating-gate slits [21].

For a strong spatial modulation of the structure, the spatial waveform of any particular plasmon mode contains all spatial Fourier harmonics with different wavevectors $q = 2\pi p/L$. Spatial waveform of a plasmon mode and its Fourier spectrum depends on the strength of spatial modulation of the 2D electron system. Figures 3a and b demonstrate the calculated spatial waveforms [35] of different plasmon modes in the grating-gate FET structure for weak (Fig. 3a) and strong (Fig. 3b) spatial modulation of the electron density in 2D electron channel described by the modulation factor defined as $\alpha = (N_2 - N_1)/(N_2 + N_1)$, where N_1 and N_2 are the values of the equilibrium 2D electron density in the channel under the grating-gate fingers and under the grating-gate openings, respectively (a rectangular spatial distribution of the equilibrium 2D electron density in the channel is assumed).

For a weak spatial modulation of the 2D electron channel, the spatial Fourier harmonic with the wavevector $2\pi m/L$ dominates in the m-th plasmon resonance, where m = 1,2,3,… is the number of the plasmon resonance in ascending order in frequency and a spatial waveform of the plasmon mode occupies the entire period of the transistor structure (see Fig. 3a). The frequency of the m-th plasmon resonance in the grating-gate transistor structure with a homogeneous (unmodulated) 2D electron channel falls in between the frequencies of the respective plasmon modes in unscreened and totally

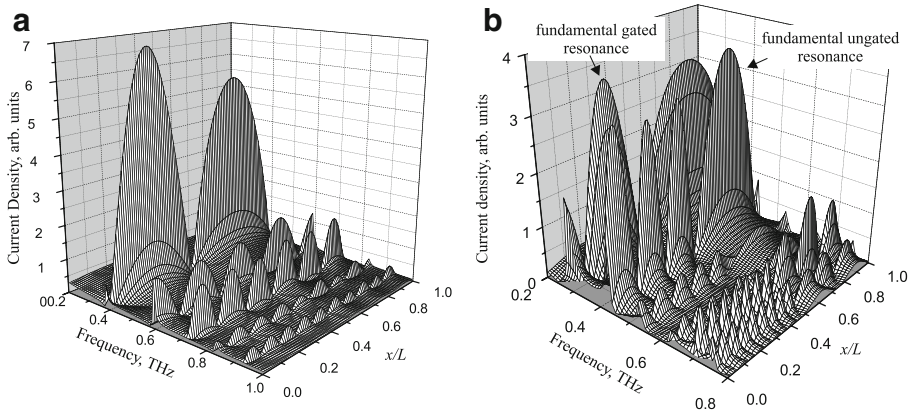

Fig. 3 Distribution of the magnitude of the oscillating electric current density in (a) unmodulated 2D electron channel (α=0) and (b) modulated 2D electron channel (α=0.43) over the period of the grating-gate AlGaAs/GaAs FET structure as a function of frequency for L=4 μm, w=2 μm, d=0.4 μm. The gated portion of 2D electron channel occupies the interval $0 < x/L < 0.5$. The electron concentration in the ungated portions of 2D electron channel is $N_2 = 2.57 \times 10^{11}\text{cm}^{-2}$ and the electron scattering rate is $\gamma_e = 1.5 \times 10^{10}\text{s}^{-1}$ (after Ref. [35]).

screened 2D electron system, which are given by Eq. (1) for $q = 2\pi m/L$ for the effective dielectric functions given by Eqs. (2) and (3), respectively.

For the arbitrary modulation factor α, the gated plasmons (localized in the FET sections under the grating-gate fingers with the wavevectors defined by the width of the grating-gate strip w) as well as the ungated plasmons (localized in the FET sections under the grating-gate openings with the wavevectors defined by the width of the slit s between the adjacent gate fingers) can be excited (Fig. 3b). The frequencies of the gated plasmon resonances in Fig. 3(b) are in good correspondence with the plasmon frequencies calculated using Eq. (1) for $q = q_m = (2m-1)\pi/w$ $(m = 1, 2, 3, ...)$ with the effective dielectric function given by Eq. (3), while the frequencies of the ungated plasmon resonances (seen at frequencies above 0.4 THz in Fig. 3b) are in good agreement with the plasmon frequencies given by Eq. (1) for $q = q_m = (2m-1)\pi/s$ with the effective dielectric function given by Eq. (2).

Because the gated plasmons are strongly screened by the gate fingers, the fundamental frequency of the gated plasmon resonance (seen at about 0.2 THz in Fig. 3b) is much lower than the frequency of the fundamental ungated plasmon resonance (exhibited at about 4.5 THz). As mentioned above, the gated and ungated plasmon modes in the grating-gate transistor structure can not exist independently of each other. Once excited, the gated plasmon modes induce forced plasma oscillations in the ungated regions of the 2D electron channel in low frequencies (see the electric current density distributions in the channel at the frequencies of the gated plasmon resonances below 0.4 THz in Fig. 3b). The ungated plasmon modes excited in frequencies above 0.4 THz induce forced plasma oscillation in the gated portions of the 2D electron channel when the ungated plasmon frequency does not coincide with the frequency of a higher-order gated plasmon mode. When the frequency of the ungated plasmon mode is close to the frequency of a higher-order gated plasmon mode, the plasmon-mode anticrossing should be exhibited. However, due to the screening of the gated portions of 2D electron channel by the gate fingers (and also due to a smaller electron density in the gated regions of the channel), different resonances of the gated plasmon modes are densely spaced in frequency and hence a particular resonance of the ungated plasmon mode is merged into a dense spectrum of the gated plasmon modes. Therefore, for a relatively strong spatial modulation of the equilibrium electron density in the channel, the ungated plasmon mode always experiences the resonant anticrossing with some gated plasmon mode. For example, one can see the interaction of the fundamental ungated plasmon mode, having the wavevector π/s, with the second gated plasmon mode, having the wavevector $3\pi/w$, at a frequency around 0.4 THz and the interaction of the second ungated plasmon mode, having the wavevector 3π/s, with the fourth gated plasmon mode, having the wavevector 7π/s, at a frequency of 0.7 THz in Fig. 3b.

It is worth mentioning that the ungated regions of the 2D electron channel are very important for effective excitation of the gated plasmon resonances in the grating-gate transistor structure with the spatially modulated 2D electron channel. Due to the oscillating charges induced by the incoming THz wave in the ends of the ungated regions of the channel, these regions act as electrical vibrators exciting the gated plasmon modes. As reported in [21], the intensity of the gated plasmon resonances decreases by two orders of magnitude in the grating-gate transistor structure with totally depleted ungated regions of the 2D electron channel. The effect of the ungated regions of the channel greatly increases at the frequencies of the ungated plasmon resonances. This effect can be used for the enhancement of the gated plasmon resonances via exciting a "firing" ungated plasmon mode at the same frequency.

In spite of the strong interaction of the gated and ungated plasmons in the grating-gate transistor structure, the linewidth of either type of the plasmon resonances is comparable with the electron scattering rate γ_e in the 2D electron system (note that, in a single-gate

transistor structure, the gated plasmon resonance linewidth can exceed the electron scattering rate by an order of magnitude [26] due to the intermode plasmon-plasmon scattering [25]). In distinction from a single-gate transistor, the interaction of the gated and ungated plasmons in the grating-gate transistor structure does not cause the plasmon resonance linewidth broadening but instead leads to the formation of a collective plasmon mode distributed over the entire area of the structure via synchronizing the plasma oscillations in all unit cells of the structure.

Another possible reason for broadening the plasmon resonance spectral line was suggested in Refs. [36] and [37]. In a single-gate FET, the gate length (which is defined by the width of the gate finger) is commonly much shorter (typically by two or even three orders of magnitude) than the width of the channel (which is dimensioned by the length of the gate finger). In such a device, a continuum of so-called oblique plasmon modes propagating along the gate finger (i.e., athwart the channel) can be supported [38], which could, in principle, broaden the plasmon resonance spectral line. However, as shown in Ref. [39], the oblique plasmon modes cannot be normally excited in the FET with a wide channel by irradiating it with THz wave (unless due to the antenna effect of peripheral metal contacts in the single-gate FET). Because a large-area grating gate with a short period acts as an effective THz-wave polarizer [40], no oblique plasmon modes can be excited in the grating-gate FET structures even by unpolarized or uncollimated THz beam unless due to small parasitic uncontrollable corrugations of the grating-gate fingers. Therefore, the excitation of the oblique plasmon mode can hardly affect the width of the plasmon resonance spectral line in the grating-gate FET structure.

Measured and calculated plasmon-resonance spectra in the AlGaN/GaN FET structure with the 2D electron channel and the grating-gate with narrow slits are shown in Figs. 4 and 5,

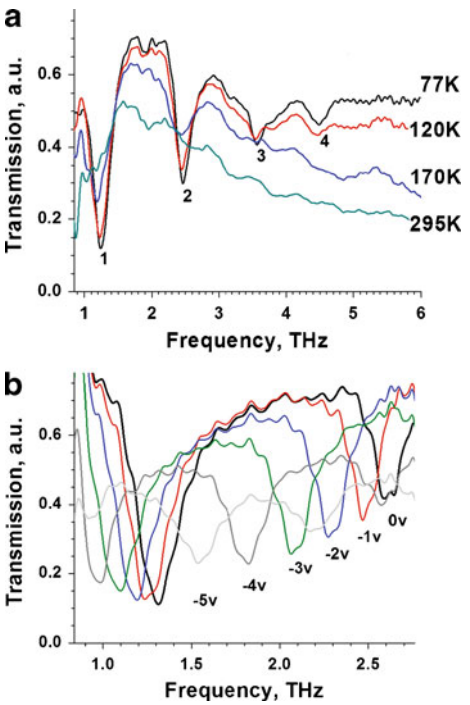

Fig. 4 (color online) (a) Transmission spectra of the slit-grating-gate AlGaN/GaN FET structure, referenced to free space, measured at temperatures from 77 K to 295 K for U_g=0. (b) Transmission spectra for different applied gate voltages U_g: 0 V; −1 V; −2 V; −3 V; −4 V; and −5 V at T=10 K. The spectra are referenced to the transmission spectrum of the identical AlGaN/GaN device without metal gate grating. The grating gate has the period 1.5 μm and slit width 0.35 μm (after Ref. [22]).

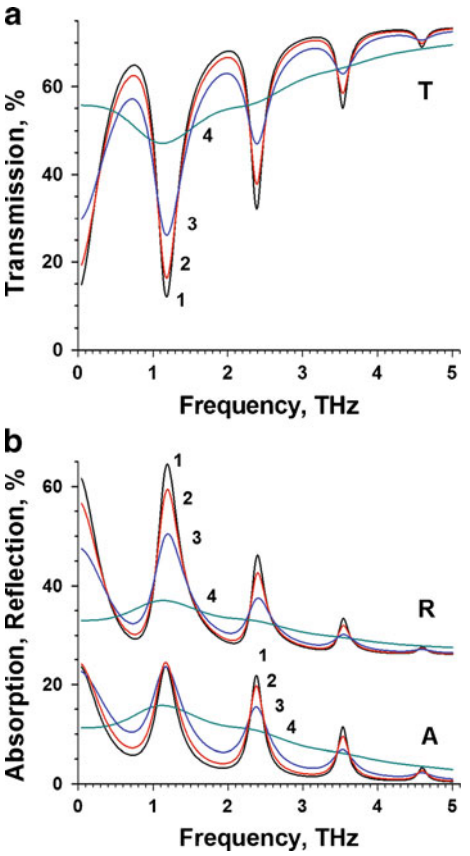

Fig. 5 (color online) (a) Calculated transmission (T) spectra of the slit-grating-gate AlGaN/GaN HEMT structure for different electron mobilities: (1) $\mu_{77\ K}$=10 000 cm^2 / V s (τ=1.14×10^{-12} s), (2) $\mu_{120\ K}$= 7600 cm^2 /V s (τ=0.86×10^{-12} s), (3) $\mu_{170\ K}$=400 cm^2 /V s (τ=0.5×10^{-12} s), and (4) $\mu_{295\ K}$= 1200 cm^2 /V s (τ=0.14×10^{-12} s). (b) Corresponding calculated absorption (A) and reflection (R) spectra. The grating gate has the period 1.5μm and slit width 0.35μm (after Ref. [22]).

respectively. Due to strong electromagnetic coupling between plasmons and THz radiation in the narrow-slit grating-gate structure, the fundamental and higher-order plasmon resonances can be excited at elevated temperatures in a broad THz frequency range.

The electromagnetic coupling of a grating-gate plasmonic detector to terahertz radiation can be considerably enhanced by placing the detector onto a thin (membrane) substrate [41]. The THz absorbance at plasmon resonance in the grating-gate FET structure is [34]

$$A_{\text{res}} = \frac{2\gamma_e\gamma_r}{(\gamma_e+\gamma_r)^2}(1-\sqrt{R_0}), \tag{7}$$

where $\gamma_e = 1/2\tau$ is the plasmon dissipative damping caused by electron scattering in the 2DEC with the characteristic relaxation time τ, R_0 is the reflectivity of a bare substrate (without the grating-gated transistor structure), and

$$\gamma_r = \beta^2 \frac{e^2\overline{N}}{2m^*} Z_{\text{eff}} \tag{8}$$

is the radiative damping of plasmons with β^2 being a phenomenological coefficient of coupling between the incident THz electromagnetic wave and the plasmon mode, $\overline{N}$ being the equilibrium sheet electron density in the 2D electron channel averaged over the period of the

structure, and Z_{eff} being the effective impedance of outside ambient. In particular, one has $Z_{\text{eff}} = Z_0/(\sqrt{\varepsilon}+1)$, where Z_0 is the free space impedance, for the grating-gate FET structure on a bulk substrate having the dielectric constant ε and $Z_{\text{eff}} = Z_0/2$ for the grating-gate FET structure on a membrane substrate.

As follows from Eq. (7), the maximal absorbance at the plasmon resonance $A_{\text{res}}^{\max} = 0.5(1-\sqrt{R_0})$ occurs for $\gamma_e = \gamma_r$. For example, for a GaAs bulk substrate (ε=12.8), one obtaines $A_{\text{res}}^{\max} \approx 0.22$. However, twice as much absorbance, $A_{\text{res}}^{\max} \approx 0.5$, can be obtained in the grating-gate FET structure on a membrane substrate due to vanishing reflectivity of the membrane substrate, $R_0 \to 0$. Radiative damping of plasmons, Eq. (8), grows by a factor of $(\sqrt{\varepsilon}+1)/2$ in the membrane structure.

The value of γ_r can be close to γ_e at the fundamental plasmon resonance in a slit-grating-gate FET structure [21]. However, the inequality $\gamma_r < \gamma_e$ is typically valid for higher-order plasmon resonances (because of a small net dipole moment of a higher-order plasmon mode). In this case, Eq. (7) becomes

$$A_{\text{res}} \approx 2\frac{\gamma_r}{\gamma_e}(1-\sqrt{R_0}). \tag{9}$$

Therefore, the absorbance at higher-order plasmon resonances given by Eq. (9) increases due to the cumulative effect of reduced reflection ($R_0 \to 0$) and enhanced radiative damping, γ_r, of plasmons in the membrane structure.

Figures 6a and b show the calculated spectra of plasmon resonances in the grating-gate AlGaAs/GaAs FET structure on the bulk and membrane substrates, respectively, for different values of the grating-gate aspect ratio w/L. In accordance with Eq. (7), the maximum absorbance at the plasmon resonance reaches $0.5(1-\sqrt{R_0}) \approx 0.22$ in the structure with a bulk GaAs substrate (see Fig. 6a) and 0.5 in the structure with a membrane substrate (Fig. 6b). As seen from Fig. 6, the absorbance at the second-order plasmon resonance increases roughly by a factor of 5 in the structure on the membrane substrate compared to the structure on a bulk substrate for the same grating aspect ratio in accordance with Eq. (9). The absorbance at the higher-order plasmon resonances increases by more than an order of magnitude for the narrow slits of the grating gate due to enhanced electromagnetic coupling between the plasmons and THz radiation.

4 Plasmon nonlinearities and THz detection in the grating-gate FET

For relatively dense 2D electron plasma, the plasmon dynamics can be described by the hydrodynamic equations for the 2D electron fluid [1, 2]

$$\frac{\partial V(x,t)}{\partial t} + V(x,t)\frac{\partial V(x,t)}{\partial x} + \frac{V(x,t)}{\tau} + \frac{e}{m^*}E(x,t) = 0, \tag{10}$$

$$e\frac{\partial}{\partial t}N(x,t) - \frac{\partial}{\partial x}j(x,t) = 0, \tag{11}$$

where $E(x,t)$ is the in-plane electric field depending on the time t and coordinate x in the 2D electron system (x-axis is directed along the periodicity of the structure), τ is the electron momentum relaxation time due to electron scattering in the 2D system, $j(x,t) = -eN(x,t)V(x,t)$ is the density of the induced electric current, $N(x,t)$ and $V(x,t)$ are the hydrodynamic electron density and velocity in the 2D electron channel.

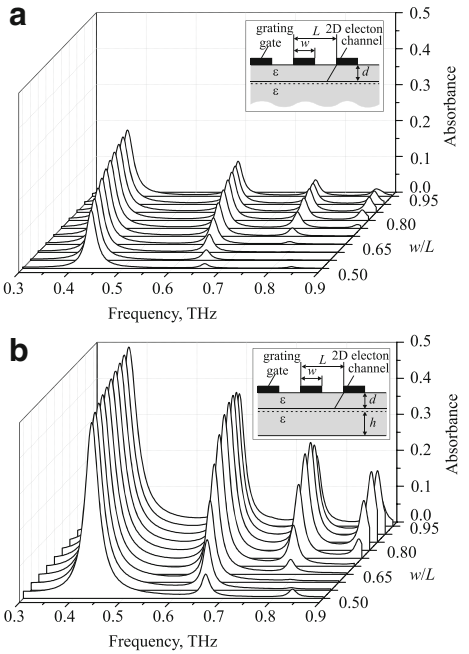

Fig. 6 Calculated THz absorption spectra of the grating-gate AlGaAs/GaAs FET structure on (a) a bulk substrate and on (b) the membrane substrate for U_g=−1 V, L=4 μm, d=0.4 μm, ε=12.8, and τ=8.5×10^{-12} s. Electron density in the channel at zero gate voltage is 4.14×10^{11} cm^{-2}. Thickness of the membrane substrate is h=4 μm. The insets in panels (a) and (b) show schematic views of the grating-gate structures on bulk and membrane substrates, respectively (after Ref. [41]).

There are two nonlinear terms in the system Eqs. (10) and (11): the second term in the Euler equation, Eq. (10), describes the nonlinear electron convection in the 2D electron fluid and the product $N(x,t)V(x,t)$ defines the current density in the continuity equation Eq. (11). The time average of the nonlinear current yields the detection signal. It should be noted that either of the two nonlinear terms vanishes in the case of a uniform oscillating current flowing in the 2D electron system. Therefore, those nonlinearities are related to non-uniform electric currents inherent in the plasma oscillations. In principle, the both nonlinear terms can contribute to the detection signal depending on the geometry of the structure. For symmetry reasons, the detection response is zero in the grating-gated FET structure with a symmetric unit cell if there is no DC bias current flowing in the channel. In a periodic structure with a homogeneous 2D electron channel, the electron convection term in the Euler equation [the second term in Eq. (10)] does not contribute to the detection signal of the entire structure incorporating many dozens of periods because the spatial average of this term over the structure period is zero. Therefore, the only source of hydrodynamic nonlinearity in the periodic structure with a homogeneous 2D electron channel is the product $N(x,t)V(x,t)$ defining the current density in 2D electron fluid. However, if the equilibrium electron density in the 2D channel varies over the structure period, the electron convection term in the Euler equation can vastly contribute to the detection signal.

In a FET with a periodic grating gate, the DC photocurrent induced in the 2D electron channel by incoming THz radiation can be calculated in the perturbation approach using the Fourier representation of Eqs. (10) and (11) [42]:

$$j_0 = -e\sum_{q\neq 0}\left(N_q^{(0)}V_{0,-q} + N_{0,q}V_{-q}^{(0)}\right) - 2e\mathrm{Re}\sum_{q\neq 0}N_{\omega,q}V_{\omega,q}^{*}, \tag{12}$$

where $N_{\omega,q}$, $V_{\omega,q}$ and $N_{0,q}$, $V_{0,q}$ are the amplitudes of the space-time Fourier harmonics of the induced electron density and velocity at the frequency ω of the incoming THz radiation

and at zero frequency, respectively, and $N_q^{(0)}$ and $V_q^{(0)}$ are the amplitudes of the spatial Fourier harmonics of the equilibrium electron density $N^{(0)}(x)$ and DC drift velocity $V^{(0)}(x)$ in the 2D electron channel (the DC drift velocity is related to the equilibrium electron density as $V^{(0)}(x) = j_{bias}/eN^{(0)}(x)$ with j_{bias} being the DC bias current density in the 2D electron channel). It is worth noting that $N_{\omega,q}$ and $V_{\omega,\mathrm{q}}$ are linear in the electric field amplitude of the incoming THz wave, while $N_{0,q}$ and $V_{0,q}$ are proportional to the second power of the electric field amplitude of incoming THz wave in the perturbation approach.

The photocurrent given by Eq. (12) is zero in the grating-gate structure with a symmetrical unit cell when there is no DC electron drift in the 2D electron channel. Therefore, THz photoresponse defined by Eq. (12) is exhibited in the grating-gate structure with a symmetrical unit cell as the THz photoconductivity effect only when a non-zero DC bias current is flowing in the 2D channel. In a 2D system with homogeneous electron density, only the second-sum term survives in the right-hand side of Eq. (12). This term describes the plasmon-driven DC electron drag in the 2D system because every qth summand in this series is proportional to the wave vector of the corresponding Fourier harmonic of the induced electric field in the 2D channel [43]. [In a grating-gate structure with a symmetrical unit cell and without DC electron drift in the 2D electron channel, the Fourier-harmonics of the electric field, which have the wave vectors of opposite signs, have equal amplitudes and hence the net electron drag effect is zero.] The first-sum term arises in Eq. (12) only if the equilibrium electron density in the 2D electron system is spatially modulated along the x-direction. This term originates from the electron convection nonlinear term in the Euler equation Eq. (10). The photocurrent described by this term can be interpreted as a result of the plasma electrostriction effect in the 2D electron system with an inhomogeneous electron density [42] since the amplitudes of the space-time Fourier harmonics of the induced electron density and velocity at zero frequency, entering the first-sum term in Eq. (12), are proportional to the second power of the electric field amplitude of the incoming THz wave.

Plasmonic detection of THz radiation in the grating-gate transistor structures was observed in [40, 44–47]. Enhanced responsivity of the grating-gate plasmonic THz detector placed on a membrane substrate was observed in Ref. [46]. In the fixed bias current regime used in experimental studies of the THz photoconductivity, the THz photoresponse manifests itself as an additional source-to-drain DC photovoltage $\delta U_0 = -j_0 D/\sigma_0$ where D is the entire channel length in the grating-gate transistor structure and σ_0 is spatially averaged DC conductivity of the channel. Figure 7 demonstrates the calculated relative photoresponse (normalized to the source-to-drain voltage drop without THz illumination) of the grating-gated AlGaAs/GaAs FET structure with the following parameters: D=2 mm, L=4 μm, the width of the grating-gate finger w=2 μm, the distance between the grating gate

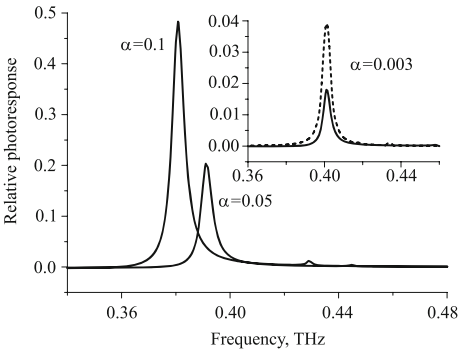

Fig. 7 Photoresponse vs frequency near the fundamental plasmon resonance for the grating-gate AlGaAs/GaAs FET structure with modulated 2D electron channel at different values of the modulation factor α for N_2=2.57×10^{11} cm^{-2} (after Ref. [42]). Dashed curve in the inset corresponds to the hot electron photoresponse at temperature 40 K.

and the 2D channel d=0.4 μm, j_{bias}=0.05 A/m, the electron scattering time in 2D channel τ=6.67×10^{-11} s, and the input THz intensity is 1 W/cm^2 for different values of the electron density modulation factor $\alpha = (N_2 - N_1)/(N_2 + N_1)$. The trapezoidal profile of the equilibrium electron density distribution $N^{(0)}(x)$ in the 2D electron channel is assumed with N_1 and N_2 being the minimal (under the grating-gate finger) and maximal (under the grating-gate opening) electron density values, respectively.

The photoresponse peak in Fig. 7 is the result of the resonant enhancement of the THz in-plane electric field in the 2D channel when the fundamental plasmon mode is excited in the 2D channel. The height of the peak strongly depends on the modulation factor. At α=0 the photoresponse is determined solely by the plasmon-driven electron drag [43]. The electron drag term practically does not depend on α, whereas the electrostriction term vastly increases in the density modulated 2D electron channel over the electron drag and electron heating contributions.

Figure 8 demonstrates the spectra of the photoconductive response of the InGaAs/GaAs transistor structure with a slit-grating gate (the ratio between the slit width and the grating-gate period is 1:10) measured at a temperature of 4.2 K (Fig. 8a) and the respective calculated plasmon absorption spectra (Fig. 8b). The detection response in the slit-grating gate FET structure [47] exceeds that in a conventional grating-gate FET [44, 45] by an order of magnitude due to enhanced coupling between plasmons and THz radiation in the slit-grating-gate structure. Although the responsivity of the grating-gate plasmonic THz

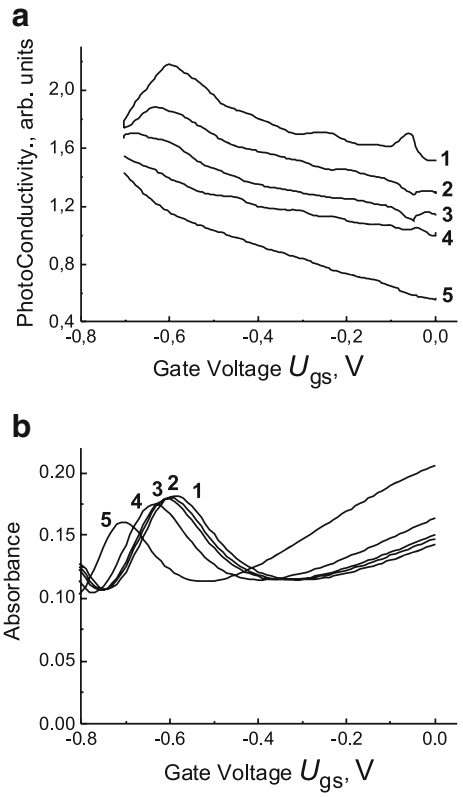

Fig. 8 Series of plots of the (a) drain-to-source photoconductivity response measured at temperature 4.2 K (for the sake of clarity, the curves are shifted along the vertical axis) and (b) calculated absorbance versus the gate voltage for the grating-gate InGaAs/GaAs transistor structure for five frequencies of the incident radiation (GHz): (*1*) 697; (*2*) 688; (*3*) 682; (*4*) 659; (*5*) 593. The grating gate has the period 3 μm and the slit width is 0.3 μm. The DC bias current in the channel is 0.5 mA (after Ref. [47]).

detector reported in Ref. [47] is still lower than the practical requirements, the steady progress in the development of this technology is very promising.

5 Conclusions

The field-effect transistor structure with the grating gate can be used for the detection of THz radiation based on hydrodynamic plasmonic nonlinearities in the 2D electron channel of the transistor structure. The grating gate of a large area (comparable with the typical cross-section area of a focused THz beam) acts as an aerial matched antenna coupling the plasmons in the transistor channel to THz radiation. The grating gate with narrow grating slits can effectively couple THz radiation to higher-order plasmon modes at high THz frequencies and elevated temperatures above the liquid nitrogen temperature. The plasmonic detection response considerably increases due to the 2D electron plasma electrostriction effect in the grating-gate FET structure with the spatially modulated electron channel. Several orders of magnitude improvement in the responsivity of the grating-gate plasmonic THz detectors as well their operation at room temperature are still necessary before such devices become viable for broad use in THz technology.

Acknowledgements This work was performed under the umbrella of the GDR-I project "Semiconductor Sources and Detectors for Terahertz Frequencies" with the support from the Russian Foundation for Basic Research (Grant Nos. 11-02-92101 and 10-02-93120) and from the Russian Academy of Sciences Program "Fundamentals of Nanotechnology and Nanomaterials". I am grateful to my colleagues Drs. M. S. Shur, W. Knap, V. I. Gavrilenko, S. J. Allen, G. R. Aizin, N. J. M. Horing, T. Otsuji, Y. M. Meziani, A. V. Muravjov, D. B. Veksler, N. Pala, D. Coquillat, F. Teppe, N. Dyakonova, D. V. Fateev, O. V. Polischuk, G. M. Tsymbalov, K. V. Marem'yanin, D. M. Ermolaev, N. A. Maleev, V. E. Zemlyakov, and S. Yu. Shapoval for their invaluable contribution to our collaborative research on THz plasmonic properties of the grating-gate transistor structures.

References

1. M. Dyakonov and M. Shur, IEEE Trans. Electron Devices **43**, 380 (1996).
2. M. S. Shur and J.-Q. Lu, IEEE Trans. Microwave Theory and Techniques **48**, 750 (2000).
3. W. Knap, J. Lusakowski, T. Parenty, S. Bollaert, A. Cappy, V. V. Popov, and M. S. Shur, Appl. Phys. Lett. **84**, 2331 (2004).
4. A. Satou, I. Khmyrova, V. Ryzhii, and M. S. Shur, Semicond. Sci. Technol. **18**, 460 (2003).
5. A. Satou, V. Ryzhii, I. Khmyrova, M. Ryzhii, and M. S. Shur, J. Appl. Phys. **95**, 2084 (2004).
6. F. Teppe, W. Knap, D. Veksler, M. S. Shur, A. P. Dmitriev, V. Yu. Kachorovskii, and S. Rumyantsev, Appl. Phys. Lett. **87**, 052107 (2005).
7. N. Pala, F. Teppe, D. Veksler, Y. Deng, M. S. Shur, and R. Gaska, Electron. Lett. **41**, 447 (2005).
8. A. El Fatimy, F. Teppe, N. Dyakonova, W. Knap, D. Seliuta, G. Valušis, A. Shchepetov, Y. Roelens, S. Bollaert, A. Cappy, and S. Rumyantsev, Appl. Phys. Lett. **89**, 131926 (2006).
9. V. I. Gavrilenko, E. V. Demidov, K. V. Marem'yanin, S. V. Morozov, W. Knap, and J. Lusakowski, Fiz. Tekh. Poluprovodn. (St. Petersburg) **41**, 238 (2007) [Semiconductors **41**, 232 (2007)].
10. W. J. Stillman and M. S. Shur, J. Nanoelectron. Optoelectron. **2**, 209 (2007).
11. A. V. Antonov, V. I. Gavrilenko, K. V. Marem'yanin, S. V. Morozov, F. Teppe, and W. Knap, Fiz. Tekh. Poluprovodn. (St. Petersburg) **43**, 552 (2009) [Semiconductors **43**, 528 (2009)].
12. A. El Fatimy, N. Dyakonova, Y. Meziani, T. Otsuji, W. Knap, S. Vandenbrouk, K. Madjour, D. Théron, C. Gaquiere, M. A. Poisson, S. Delage, P. Prystawko, and C. Skierbiszewski, J. Appl. Phys. **107**, 024504 (2010).
13. A. Lisauskas, W. von Spiegel, S. Boubanga-Tombet, A. El Fatimy, D. Coquillat, F. Teppe, N. Dyakonova, W. Knap, and H. G. Roskos, Electron. Lett. **44**, 408 (2008).
14. A. El Fatimy, J. C. Delagnes, A. Younus, E. Nguema, F. Teppe, W. Knap, E. Abraham, and P. Mounaix, Opt. Commun. **282**, 3055 (2009).

15. A. Lisauskas, U. Pfeiffer, E. Öjefors, P. Haring Bolìvar, D. Glaab, and H. G. Roskos, J. Appl. Phys. **105**, 114511 (2009).
16. W. Knap, M. Dyakonov, D. Coquillat, F. Teppe, N. Dyakonova, J. Łusakowski, K. Karpierz, M. Sakowicz, G. Valusis, D. Seliuta, I. Kasalynas, A. El Fatimy, Y. M. Meziani, and T. Otsuji, J. Infrared Millim. Terahertz Waves **30**, 1319 (2009).
17. V. M. Muravev, I. V. Kukushkin, J. Smet, and K. von Klitzing, Pis'ma v Zh. Eksper. Teor. Fiz. **90**, 216 (2009) [JETP Letters **90**, 197 (2009)].
18. S. J. Allen, Jr., D. C. Tsui, and R. A. Logan, Phys. Rev. Lett. **38**, 980 (1977).
19. T. N. Theis, J. P. Kotthaus, and P. J. Stiles, Solid State Commun. **24**, 2737 (1977).
20. T. N. Theis, Surface Science **98**, 515(1980).
21. V. V. Popov, M. S. Shur, G. M. Tsymbalov, and D. V. Fateev, Int. J. High Speed Electronics and Systems **17**, 557 (2007).
22. A. V. Muravjov, D. B. Veksler, V. V. Popov, O. V. Polischuk, N. Pala, X. Hu, R. Gaska, H. Saxena, R. E. Peale, and M. S. Shur, Appl. Phys. Lett. **96**, 042105 (2010).
23. A. V. Chaplik, Surf. Sci. Reports **5**, 289 (1985).
24. V. V. Popov, A. N. Koudymov, M. Shur, and O. V. Polischuk, J. Appl. Phys. **104**, 024508 (2008).
25. V. V. Popov, O. V. Polischuk, and M. S. Shur, J. Appl. Phys. **98**, 033510 (2005).
26. V. V. Popov, O. V. Polischuk, W. Knap, and A. El Fatimy, Appl. Phys. Lett. **93**, 263503 (2008).
27. L. Zheng, W. L. Schaich, and A. H. MacDonald, Phys. Rev. B **41**, 8493 (1990).
28. C. D. Ager, R. J. Wilkinson, and H. P. Hughes, J. Appl. Phys. **71**, 1322 (1992).
29. O. R. Matov, O. F. Meshkov, O. V. Polischuk, and V. V. Popov, Int. J. Infrared and Millimeter Waves **14**, 1455 (1993).
30. R. J. Wilkinson, C. D. Ager, T. Duffield, H. P. Hughes, D. G. Hasko, H. Ahmed, J. E. F. Frost, D. C. Peacock, D. A. Ritchie, and G. A. C. Jones, J. Appl. Phys. **71**, 6049 (1992).
31. C. D. Ager and H. P. Hughes, Sol. St. Commun. **83**, 627 (1992).
32. O. R. Matov, O. F. Meshkov, and V. V. Popov, Zh. Eksp. Teor. Fiz. **113**, 988 (1998) [JETP **86**, 538 (1998)].
33. O. R. Matov, O. V. Polischuk, and V. V. Popov, Zh. Eksp. Teor. Fiz. **122**, 586 (2002) [JETP **95**, 505 (2002)].
34. V. V. Popov, O. V. Polischuk, T. V. Teperik, X. G. Peralta, S. J. Allen, N. J. M. Horing, and M. C. Wanke, J. Appl. Phys. **94**, 3556 (2003).
35. D. V. Fateev, V. V. Popov, and M. S. Shur, Fiz. Tekh. Poluprovodn. (St. Petersburg) **44**, 1455 (2010) [Semiconductors **44**, 1455 (2010)].
36. A. Shchepetov, C. Gardès, Y. Roelens, A. Cappy, S. Bollaert, S. Boubanga-Tombet, F. Teppe, D. Coquillat, S. Nadar, N. Dyakonova, H. Videlier, W. Knap, D. Seliuta, R. Vadoclis, and G. Valušis, Appl. Phys. Lett. **92**, 242105 (2008).
37. S. Boubanga-Tombet, F. Teppe, D. Coquillat, S. Nadar, N. Dyakonova, H. Videlier, W. Knap, A. Shchepetov, C. Gardès, Y. Roelens, S. Bollaert, D. Seliuta, R. Vadoclis, and G. Valušis, Appl. Phys. Lett. **92**, 212101 (2008).
38. M. I. Dyakonov, Fiz. Tekh. Poluprovodn. (St. Petersburg) **42**, 998 (2008) [Semiconductors **42**, 984 (2008)].
39. V. V. Popov, Appl. Phys. Lett. **93**, 083501 (2008).
40. D. Coquillat, S. Nadar, F. Teppe, N. Dyakonova, S. Boubanga-Tombet, W. Knap, T. Nishimura, Y.M. Meziani, T. Otsuji, V. V. Popov, and G. M. Tsymbalov, Optics Express **18**, 6024 (2010).
41. V. V. Popov, D. V. Fateev, O. V. Polischuk, and M. S. Shur, Optics Express **18**, 16771 (2010).
42. G. R. Aizin, D. V. Fateev, G. M. Tsymbalov, and V. V. Popov, Appl. Phys. Lett. **91**, 163507 (2007).
43. G. R. Aizin, V. V. Popov, and O. V. Polischuk, Appl. Phys. Lett. **89**, 143512 (2006).
44. X. G. Peralta, S. J. Allen, M. C. Wanke, N. E. Harff, J. A. Simmons, M. P. Lilly, J. L. Reno, P. J. Burke, and J. P. Eisenstein, Appl. Phys. Lett. **81**, 1627 (2002).
45. E. A. Shaner, M. Lee, M. C. Wanke, A. D. Grine, J. L. Reno, and S. J. Allen, Appl. Phys. Lett. **87**, 193507 (2005).
46. E. A. Shaner, M. C. Wanke, A. D. Grine, S. K. Lyo, J. L. Reno, and S. J. Allen, Appl. Phys. Lett. **90**, 181127 (2007).
47. K. V. Marem'yanin, D. M. Ermolaev, D. V. Fateev, S. V. Morozov, N. A. Maleev, V. E. Zemlyakov, V. I. Gavrilenko, V. V. Popov, and S. Yu. Shapoval, Pis'ma v Zh. Tekh. Fiz. (St. Petersburg) **36** (8), 39 (2010) [Tech. Phys. Lett. **36**, 365 (2010)].